Remote Sens. **2013**, *5*, 3681-3700; doi:10.3390/rs5083681

OPEN ACCESS

Remote Sensing

ISSN 2072-4292

www.mdpi.com/journal/remotesensing

Article

Slope Stability Assessment of the Sarcheshmeh Landslide, Northeast Iran, Investigated Using InSAR and GPS Observations

Mehrdad Akbarimehr [1,*], Mahdi Motagh [2] and Mahmud Haghshenas [1]

[1] Department of Surveying and Geomatics Engineering, University of Tehran, Tehran 14395-515, Iran; E-Mail: m.haghshenas@ut.ac.ir

[2] Helmholtz Centre Potsdam GFZ German Research Centre for Geosciences, D-14473 Potsdam, Germany; E-Mail: motagh@gfz-potsdam.de

* Author to whom correspondence should be addressed; E-Mail: m.akbarimehr@ut.ac.ir; Tel.: +98-21-8800-8841; Fax: +98-21-8800-8837.

Received: 29 May 2013; in revised form: 17 July 2013 / Accepted: 17 July 2013 / Published: 25 July 2013

Abstract: The detection and monitoring of mass movement of susceptible slopes plays a key role in mitigating hazards and potential damage associated with creeping slopes and landslides. In this paper, we use observations from both Interferometric Synthetic Aperture Radar (InSAR) and Global Positioning System (GPS) to assess the slope stability of the Sarcheshmeh ancient landslide in the North Khorasan province of northeast Iran. InSAR observations were obtained by the time-series analysis of Envisat SAR images covering 2004–2006, whereas repeated GPS observations were conducted by campaign measurements during 2010–2012. Surface displacement maps of the Sarcheshmeh landslide obtained from InSAR and GPS are both indicative of slope stability. Hydrogeological analysis suggests that the multi-year drought and lower than average precipitation levels over the last decade might have contributed to the current dormancy of the Sarcheshmeh landslide.

Keywords: landslide; slope stability; displacement; InSAR; GPS

1. Introduction

Landslides are one of the most destructive natural hazards that threaten human lives and influence the socioeconomic condition of many countries. A landslide is basically identified as slope failure that

is caused by gravitational force as the primary factor [1]. Other triggering factors, such as rainfall, earthquakes, floods or human activity may also influence the occurrence of this geologic event. Because of its specific geologic, morphologic, climatic and tectonic settings, Iran is one of the most landslide-prone areas in the world. By the year 2000, approximately 2600 landslides, which were responsible for 162 deaths, 176 fully destroyed houses and 170 damaged roads, were detected and mapped by experts from various government agencies in the country [2]. Figure 1 shows a landslide distribution map of Iran. As shown in Figure 1, most of the landslides are concentrated on the rim of the Alborz and Zagros mountains.

Figure 1. Landslide distribution map of Iran [3].

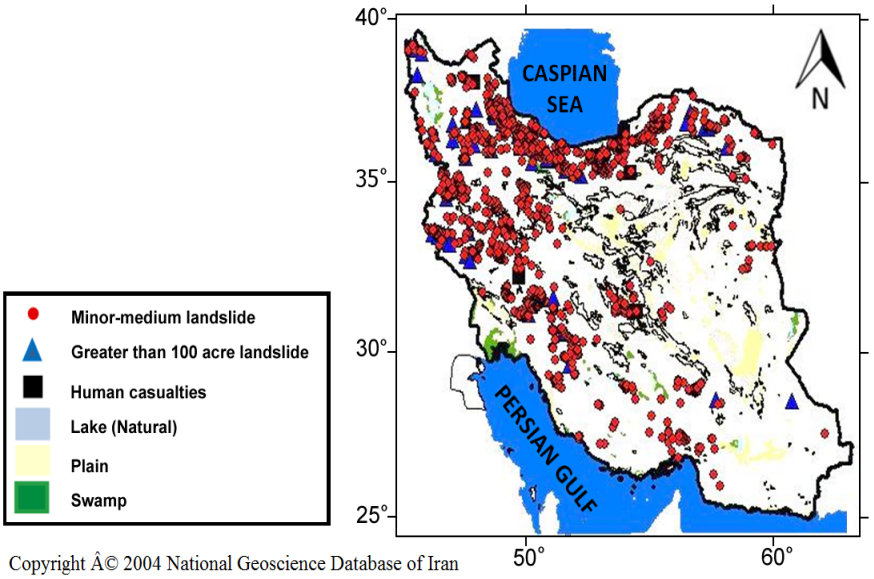

Detection and monitoring of landslides is necessary to decrease and mitigate associated losses. However, this is challenging in slow-moving landslides because of their complicated mechanisms [4]. Measurement of the surface displacement is also important to predict models of slope failure and to make risk assessments. Remote satellite techniques and *in situ* field observations are common methods to investigate landslides and monitor slope instability [5–11]. In the present study, we use Interferometric Synthetic Aperture Radar (InSAR) and Global Positioning System (GPS) observations to investigate the slope stability of the Sarcheshmeh landslide, northeast Iran.

The Sarcheshmeh landslide is a northwesterly-directed slope in the province of North Khorasan in northeastern Iran (Figure 2). A village called Sarcheshmeh with approximately 400 inhabitants is at the foot of this slope, which is 1.6 km long in the east-west direction and 600 m long in the north-south direction, with an approximate area of 100 acres.

The area has an annual precipitation of approximately 300 mm, which occurs during rainy periods from September to April [12], resulting in a relatively high level of groundwater resulting in springs on the slope (Figure 3b). The materials involved in sliding are mixtures of soil and rocks in alternating formations of thin-bedded to massive silt clay and limestone; the latter constitutes the majority of the surface geology in northeast Iran (Figure 2b). The general morphology of the study area is dominated by a mountainous landscape, which includes V-shaped valleys. Preliminary geomorphological analysis suggests that the Sarcheshmeh slope was part of a greater ancient landslide with a depth of

approximately 15 m that sustained more than 10 m downward movement [13]. Numerous scarps and bluffs with height differences ranging from 2 to 30 m are indicative of the ancient activity of this landslide (Figure 3c). All the current information about the Sarcheshmeh landslide is derived from morphological and surface geology analysis. The current rates of motion are not well known and the creeping mechanism is poorly understood. Because of the placement of the residential area, which is just downstream of the Sarcheshmeh landslide, monitoring is essential to assess the progressive deformation of this potentially dangerous slope and to avoid or mitigate any damage caused by sudden slope failure. Because of the complicated nature of the landslide phenomenon, information about the previous activity of the slope could help us better recognize effective components that are involved in probable slope creeping. Thus, we can benefit from InSAR techniques and extensive archives of SAR data that could assist us in studying and analyzing past mechanisms of slope motion. Additionally, to assess the current rate of deformation on the Sarcheshmeh landslide, we benefitted from the use of GPS geodetic measurements with point-wise reliable results.

Figure 2. Geology map of the study area: (**a**) Provincial map showing the location of the North Khorasan province (the green area); (**b**) surface geological map of the North Khorasan province with the location of the Sarcheshmeh slope marked by the black rectangle [14]; (**c**) outline of the Sarcheshmeh slope; the black arrows show the main direction of potential motion.

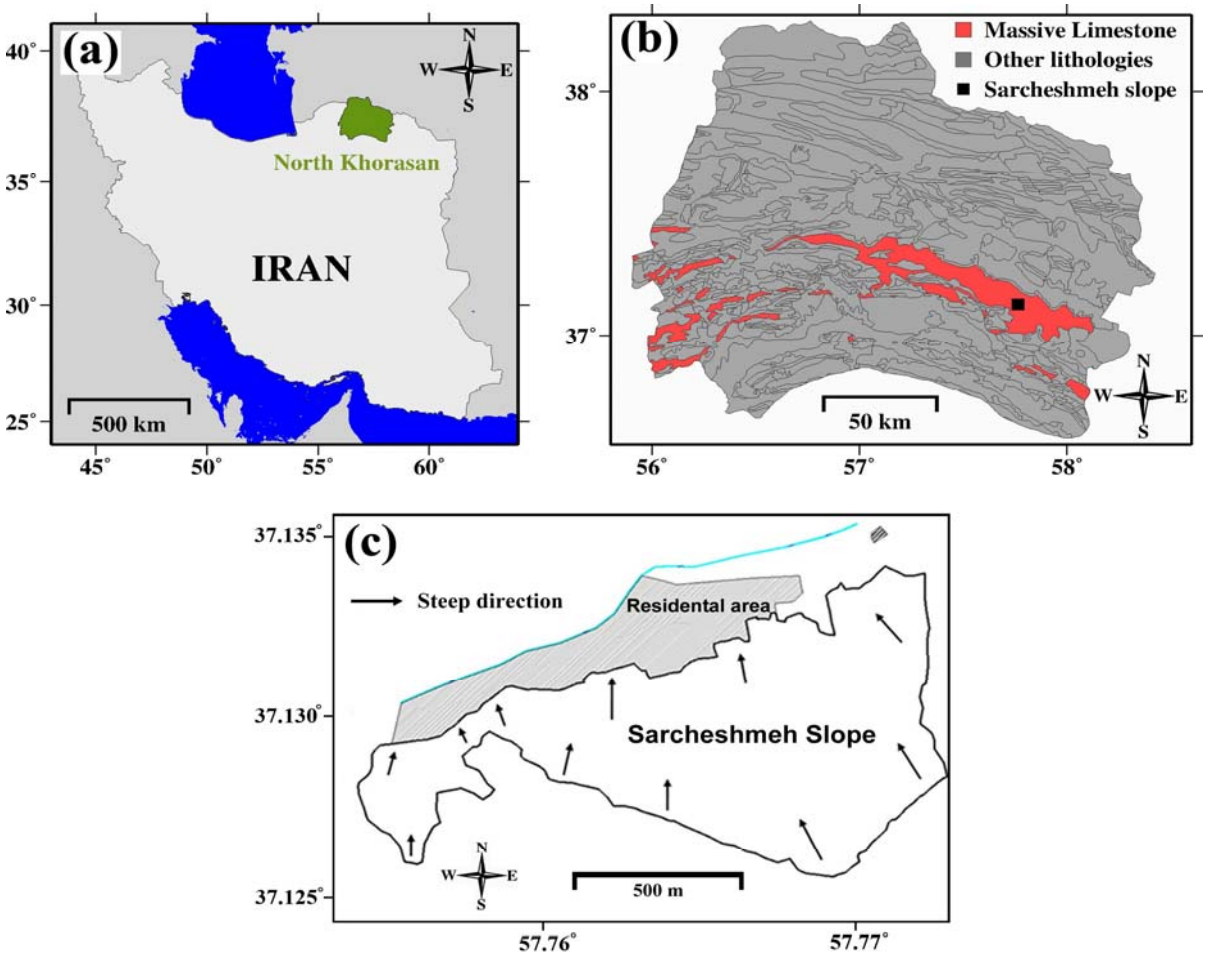

Figure 3. (**a**) A panorama photo from the north toward the study slope, which is approximately indicated by the red line; (**b**) a close-up view from the south and upper part toward the north and down the slope. Cluttered topography is obviously depicted in the photo. Additionally, two natural springs and a deep track, which was created by water erosion, are shown on this slope; (**c**) a close-up view from the west to a scarp on the slope, which is formed as a result of former activity from the landslide.

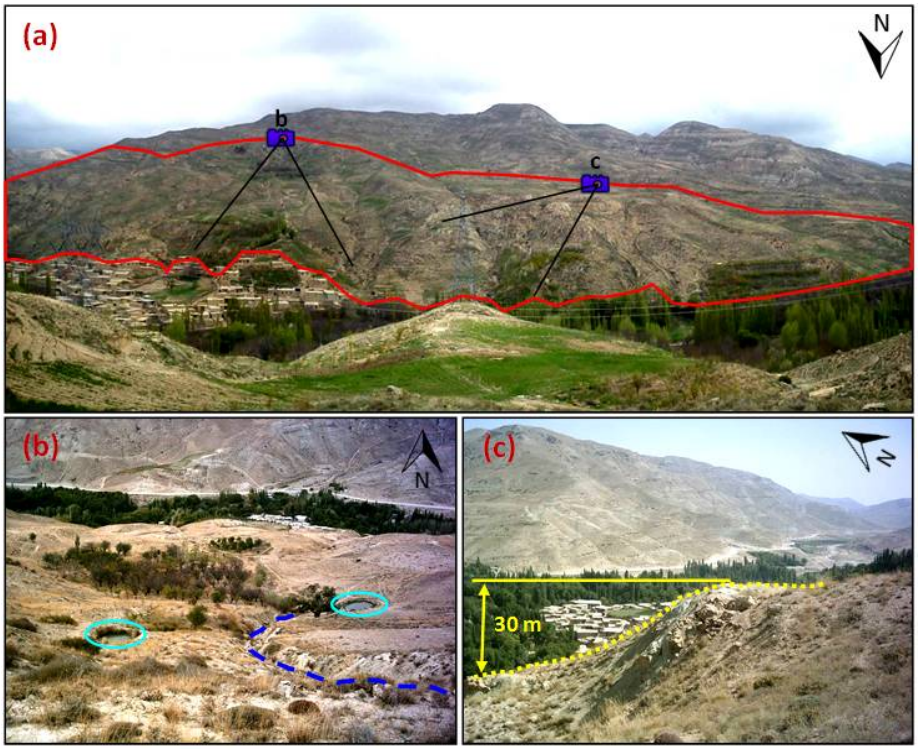

2. Data and Methodology

The dataset used in this paper is divided into two categories: SAR satellite images and GPS observations. To evaluate and analyze the past mechanisms of Sarcheshmeh surface deformation, we used the SAR interferometry (InSAR technique). The current rate of deformation was investigated using GPS periodic measurements.

Space-borne Interferometric Synthetic Aperture Radar (InSAR) has developed rapidly over the past 20 years and has proven to be a valuable tool for topographic mapping and surface deformation measurements [15,16]. Because of its dense spatial coverage and competitive accuracy, InSAR has now become one of the most preferred geodetic methods to study surface deformation associated with slow-moving landslides [17–20]. Advanced InSAR methods such as Persistent Scatterer (PS) [4,21–23] and Small Baseline Subset (SBAS) [24–26], which can overcome artifacts arising from atmospheric noise and temporal and spatial baseline decorrelation, enable us to benefit from displacement time-series analysis using a stack of SAR data. Both techniques work better in urban areas because of the high density of man-made objects, which increase the likelihood of finding coherent pixels in a stack of SAR data over time. Because of the non-urban nature of the landslide area in Sarcheshmeh (it is covered partially with grass and other permanent vegetation and used for farming), we used the SBAS technique for surface displacement time-series analysis. The SBAS method uses all possible

interferograms with a perpendicular and temporal baseline below a certain threshold to minimize decorrelation effect and topographic errors. The SBAS interferograms are then inverted after phase unwrapping for deformation time series retrieval.

GPS is a high precision positioning technique, which can be used to provide point-wise, semi-continuous maps of crustal deformation that is associated with geophysical phenomena using a variety of static or kinematic techniques [27]. Due to operating in all weather conditions and independent of direct visibility between stations and 3D precise positioning of specified points, GPS positioning is a beneficial tool in landslide monitoring [28–30]. This technique also has limitations, such as choosing the appropriate location for stations so that they have good sky views and are less affected by multipaths [27]. The choice of the observation mode and processing techniques depends on several practical considerations, such as the accessibility, cost, number of points and required precision [27].

Both GPS and InSAR are complementary to one other in that GPS provides detailed ground-truth vector information of displacement for specific localities compared to the extensive spatial coverage provided by InSAR line-of-sight (LOS) observations [31–33]. A combination of different ground and space-based geodetic monitoring systems provides promising tools to assess and evaluate geological hazards [31,32].

2.1. InSAR Analysis

For this study we used ASAR images acquired over the study area by the Envisat satellite from the European Space Agency (ESA). Sixteen descending images (Figure 4) in I2 mode (incidence angle 23°) were obtained for Sarcheshmeh spanning the years 2004–2006 (Table 1). The data were processed using the time-series approach of Small Baseline Subset (SBAS) in a two-step process: We initially produced a network of small baseline differential interferograms and subsequently did the time-series analysis to derive a one-dimensional Line-of-Sight (LOS) time-series and displacement map of surface deformation on the slope.

Figure 4. The study area in northeastern Iran (upper inset); the red box delineates the area covered by the Envisat frame in this study. Approximate location of the Sarcheshmeh landslide is specified by a black ellipse.

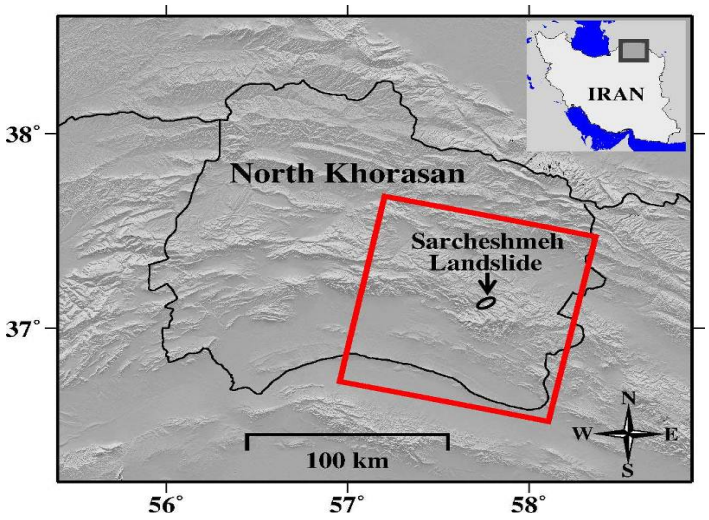

Table 1. List of used Envisat SAR images, date of acquisition and other specifications.

No	Acquisition Date	Mission	Sensor	Orbit	Track	Pass
1	2004.03.23	Envisat	ASAR	10781	206	Descending
2	2004.06.01	Envisat	ASAR	11783	206	Descending
3	2004.09.14	Envisat	ASAR	11783	206	Descending
4	2004.10.19	Envisat	ASAR	13787	206	Descending
5	2004.11.23	Envisat	ASAR	14288	206	Descending
6	2004.12.28	Envisat	ASAR	14789	206	Descending
7	2005.02.01	Envisat	ASAR	15290	206	Descending
8	2005.03.08	Envisat	ASAR	15791	206	Descending
9	2005.04.12	Envisat	ASAR	16292	206	Descending
10	2005.05.17	Envisat	ASAR	16793	206	Descending
11	2005.06.21	Envisat	ASAR	17294	206	Descending
12	2005.07.26	Envisat	ASAR	17795	206	Descending
13	2005.08.30	Envisat	ASAR	18296	206	Descending
14	2005.10.04	Envisat	ASAR	18296	206	Descending
15	2005.11.08	Envisat	ASAR	19298	206	Descending
16	2006.02.21	Envisat	ASAR	20801	206	Descending

The interferometric processing was performed using a standard repeat-pass method implemented in DORIS software, developed by the Delft Institute for Earth-Oriented Space Research (DEOS), Delft University of Technology, which is freely available to the public [34].

Figure 5. The Small Baseline (SBAS) network of selected interferograms used for the time-series analysis; horizontal and vertical axes represent the temporal and spatial baselines of selected pairs, respectively.

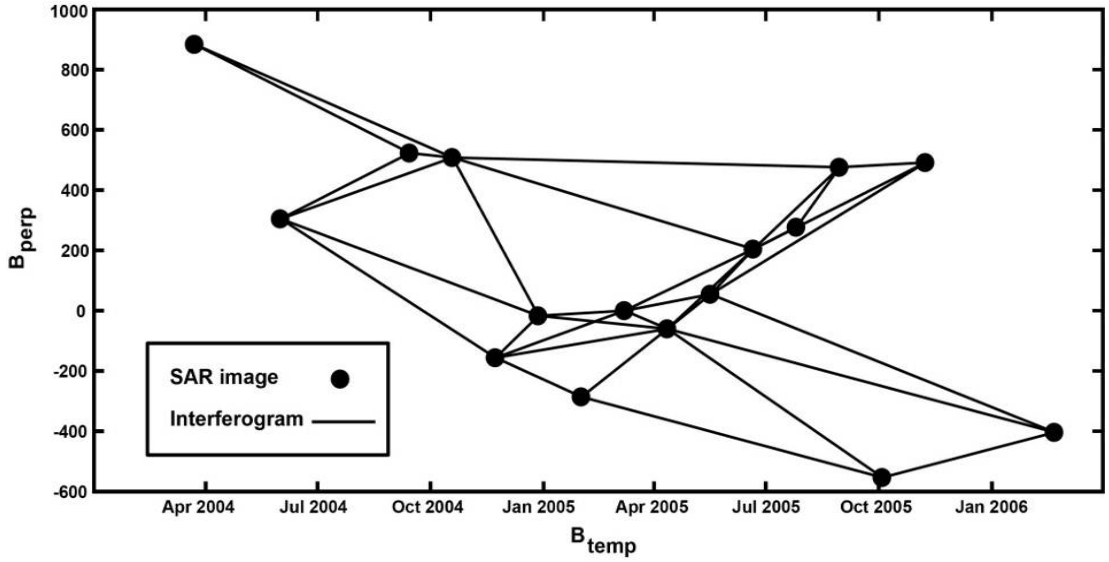

The topography-related phase correction and geocoding of the interferograms in the interferometric processing were estimated using a three arcsec Digital Elevation Model (DEM) from the Shuttle Radar Topography Mission [35]. The DEOS precise orbital information of Envisat that was estimated from the DORIS instruments provided by ESA was used during processing to eliminate orbital phase distortion [36]. We primarily formed 41 interferograms for Sarcheshmeh and then used 34 with a

maximum temporal baseline of 311 days and a perpendicular baseline of 494 m for the time-series analysis. The time-series analysis was conducted using the Small Baseline (SBAS) approach that is implemented in StaMPS software [21,22,37]. Figure 5 presents the final network of interferograms used in the SBAS processing.

2.2. GPS Analysis

To evaluate current surface deformation, we used GPS and created a geodetic network of ~20 stations, including reference and monitoring points in and around the landslide area. Constructed stations are pillars made of reinforced concrete, anchored to a depth of 1 m. The top of the pillars was 0.5 m above the ground. The reference network consists of three pillars constructed on stable localities from the geological perspective, such as bedrock around and outside the landslide area (marked as BM1, BM2, and BM3 in Figure 6). The monitoring stations were distributed near the cracks and sliding masses inside the landslide area (MP1-MP17 in Figure 6). The required accuracy for monitoring slow movement phenomena such as creeping landslides should be on the order of centimeters to millimeters [29]. GPS relative positioning in static mode can achieve millimeter accuracy after considering measuring system error sources [28]. In this study the GPS field observations were conducted in static mode with four Trimble dual frequency GPS receivers. Four campaigns of GPS field measurements were performed in October 2010, May and August 2011 and April 2012 to derive the contemporary rate of surface deformation on the Sarcheshmeh slope. Figure 6 shows the established network of control and monitoring stations on a 3D topographic map of the area.

Figure 6. The spatial distribution of Global Positioning System (GPS) stations used in this study, overlaid on a 3D view of the topography map with 1 m contour interval.

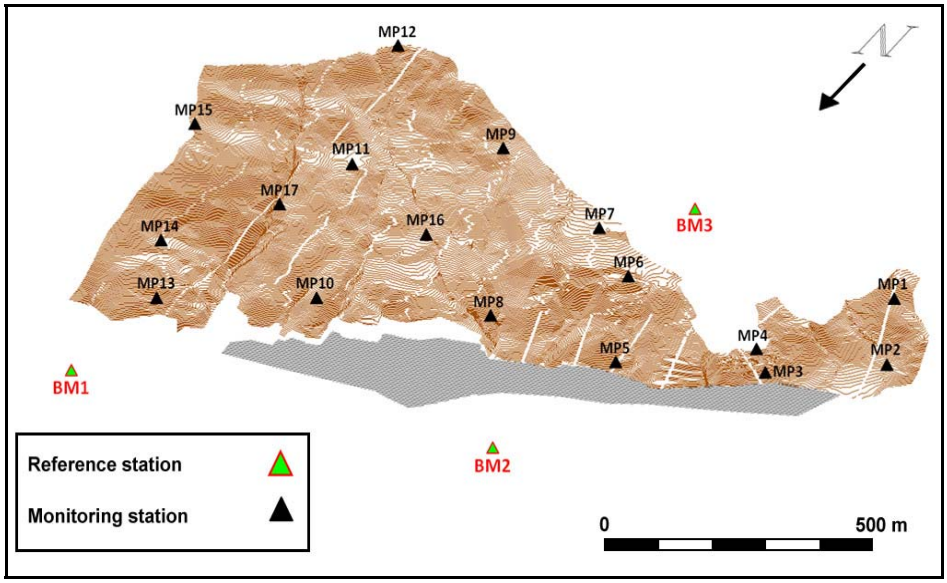

GPS observations were performed in static mode, in which monitoring points were positioned by the differential method with respect to reference points. Each monitoring point was observed from at least two reference stations. Additional observations allowed us to control the position of monitoring stations to detect any probable errors. The average session duration for baseline determination between

reference points was approximately 7 h, whereas the session duration for the baselines between the monitoring and reference points was 40 min. The collected raw data in each epoch of observation after converting to standard RINEX format were post-processed to achieve geodetic baselines between stations from space baselines between stations and satellites using precise ephemeris [38]. Figure 7 presents the final network of baselines used for positioning computation using GPS. To obtain compatibility of coordinates with the Iranian National Geodetic Network (INGN), we connected our network to a nearby permanent station from this network. A least-squares optimization method was then applied to adjust the network to determine the unique precise coordinates of stations during each campaign. It should be noted that reference network adjustment computation (baselines between reference stations BM1–BM3) was performed first in each epoch to ensure the stability of reference stations between two sequential campaigns. The displacements of the monitoring stations were computed from the difference between the coordinates of monitoring points determined in each epoch. The standard error analysis using a 95% confidence interval was applied to calculate the relative error ellipse and other statistical parameters that were associated with displacements using a variance-covariance matrix of observed baselines. It is worth nothing that computed formal errors by GPS software are usually over-optimistic [39]. Therefore a scale factor was computed and applied to the formal GPS errors based on the average of the weighted root-mean-square residual to the linear fit, computed for all stations [40–42].

Figure 7. Schematic view of GPS network observations: black lines represent intersectional considering baselines between stations.

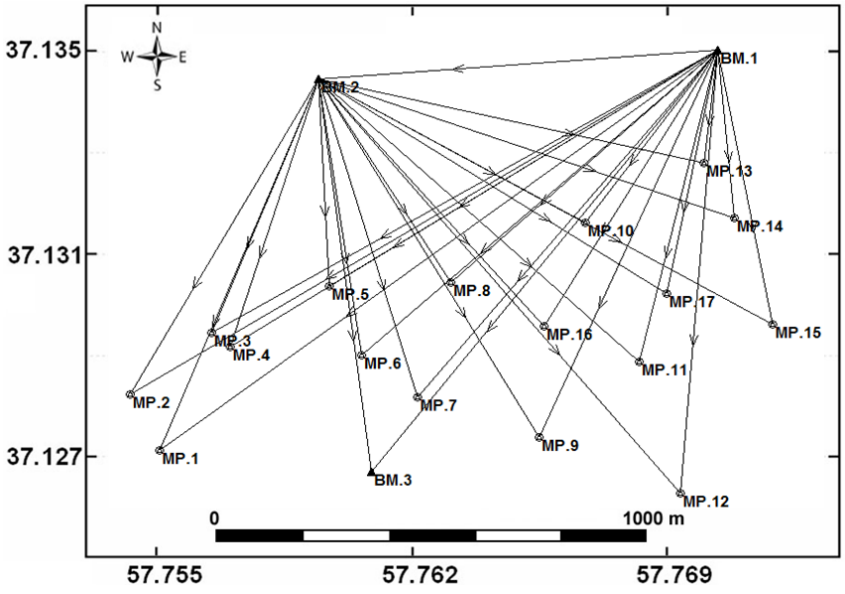

3. Results

3.1. InSAR Results

Figure 8 illustrates several differential interferograms with good coherency in geographical coordinates after removing the orbital and topography effects. Black dotted ellipses specify the Sarcheshmeh slope on the interferograms. As observed in Figure 8, short and long-wavelength

disturbances that may have arisen from tropospheric artifacts are easily recognizable in the interferograms, in turn making the estimation of slow creep signal using differential interferograms challenging. If there had been any major rapidly completed sliding process or sudden surface collapse during the observation period in Sarcheshmeh, it would have created either large-scale phase distortion or phase decorrelation in individual short-term interferograms, a pattern which was not observed either in the analyzed interferograms or during the field check-ups. However, because of atmospheric artifacts, it is difficult to evaluate the exact amount of long-term creep rate on the entire slope using only classical repeat-pass interferometry. Therefore, we focused on time-series analysis to precisely determine the rate of displacement during 2004–2006.

Figure 8. An example of four geocoded differential interferograms from the cropped part of SAR data after removing orbital and topography effects; black dotted ellipses indicate the location of Sarcheshmeh slope in the interferograms. One full color cycle, representing a difference in phase of −π to π, corresponds to 2.8 cm of LOS range change.

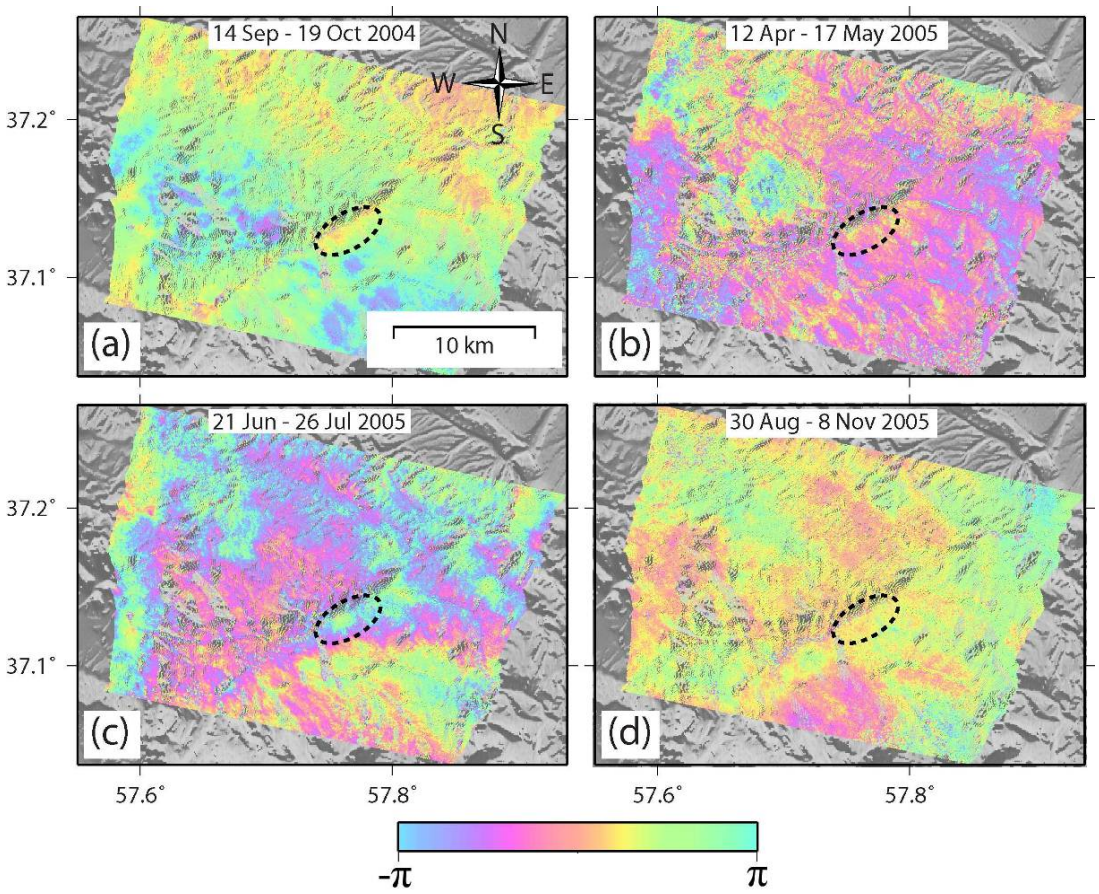

Using time-series analysis enables us to benefit from a tangible reduction in atmospheric artifact effects by averaging generated interferograms and forming a continuous surface deformation map. Figure 9a,b shows the mean velocity map of the Sarcheshmeh landslide in oblique geometry from the front view toward the slope and orthogonal geometry, respectively. The InSAR time-series analysis of the Envisat data detects more than 600 pixels that remain coherent during the time-interval covered by the Envisat data and can therefore be used for the displacement analysis. The mean deformation rate of

the slope with respect to the reference area selected on the residential area downslope is estimated at 1.2 ± 4 mm/year.

To better illustrate the time evolution of surface deformation, we selected 11 points (triangular points marked in Figure 9b) and plotted their time-series (Figure 10). These points are selected close to the GPS stations to enable comparison with the current rates of deformation at these localities. For the sake of brevity, we only demonstrate the time-series plots at TS8, TS9, TS10 and TS17 in Figure 10 and list the complete results in Table 2. As shown in Figure 10, we did not observe a significant downward trend that is indicative of slope motion in the time-series plots. All of the selected points show a dominant flat trend punctuated in time by atmospheric turbulence. Time-series analysis reveals that the displacement of the slope is lower than the error threshold of the InSAR time-series. The average standard deviation of the mean deformation velocity for points presented in Table 2 is approximately 4 mm/year. Slight fluctuations of the time-series diagram in Figure 10 are also unavoidable because of tropospheric residual errors.

Figure 9. (**a**) Mean velocity map of the Sarcheshmeh slope in oblique geometry derived from InSAR time-series analysis; (**b**) a close up view of the mean velocity map in geographical coordinates; selected points for the time-series analysis are indicated by bold triangular points and a reference point is indicated by a bold rectangular point.

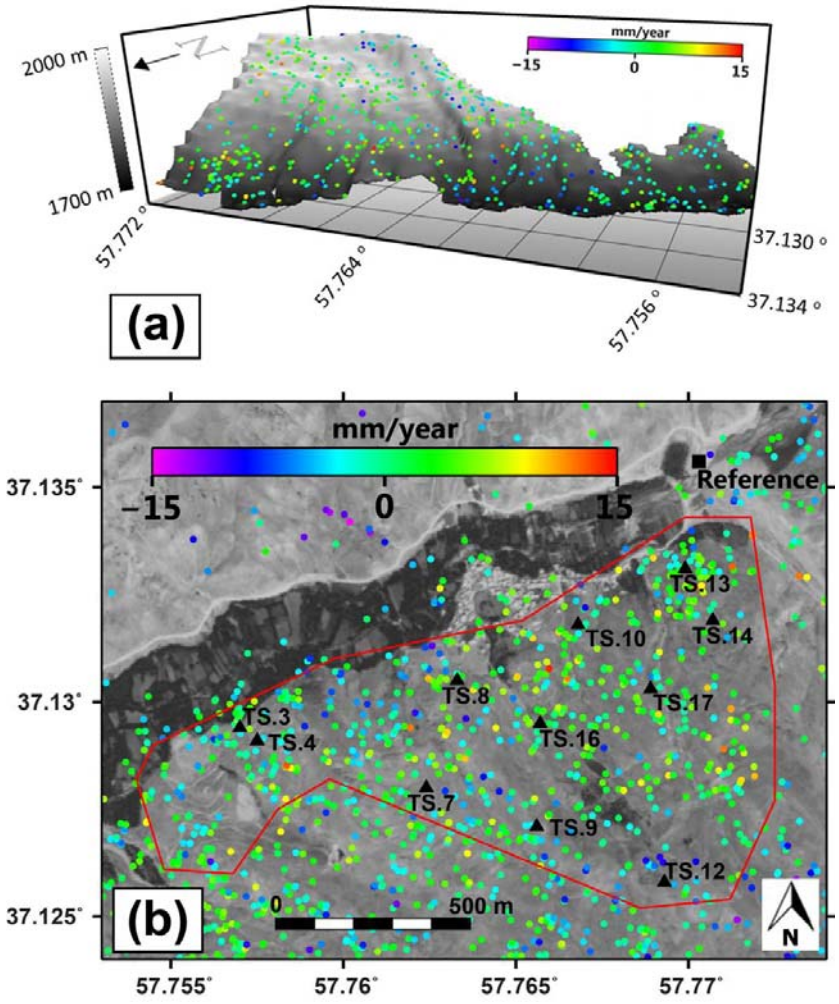

Figure 10. Four samples of InSAR time-series diagrams at TS8, TS9, TS10 and TS17; for the location of the points, please see Figure 9b. The solid circles on the diagrams represent the displacement values and the dashed red line is a one-dimensional polynomial trend fitted to displacement values. The displacement values and error bars have been computed for a window size of 100 m centered on each pixel.

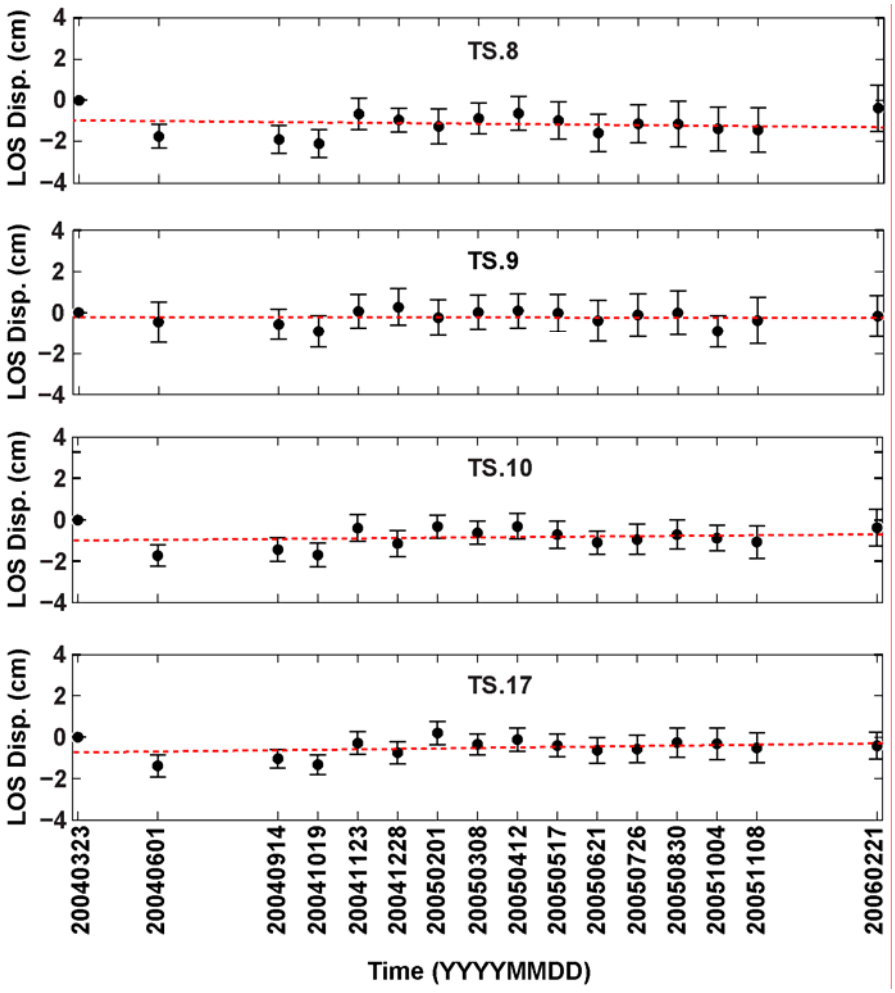

Table 2. Statistical results that were extracted from InSAR time-series analysis, which was applied for selected points in Figure 9b (displacements are in the line-of-sight (LOS) direction).

Point Name	Disp. Velocity (cm/year)	Standard Deviation (cm/year)
TS.3	0.1	±0.4
TS.4	0.1	±0.4
TS.7	0.2	±0.4
TS.8	0.2	±0.5
TS.9	0.0	±0.4
TS.10	0.2	±0.4
TS.12	−0.4	±0.5
TS.13	0.3	±0.4
TS.14	0.2	±0.4
TS.16	0.2	±0.4
TS.17	0.2	±0.3

3.2. GPS Results

Because GPS supplies a higher degree of horizontal accuracy than vertical accuracy [27], displacement results from GPS measurements are just computed and investigated for a 2D horizontal network to assess the current rate of deformation on the Sarcheshmeh landslide. Table 3 shows the numerical results for the horizontal displacement of the reference stations after four epochs of campaign measurements. Among the three reference stations, BM1 and BM2 did not show statistically significant motion during four epochs of observations and the recorded displacements between the sequential campaigns were lower than the computed standard errors. This indicates that these reference stations are on stable ground and that the difference between corresponding coordinate components in sequential epochs results from stochastic error originating from various GPS environmental and instrumental sources of errors [27]. However, for the reference stations BM3, we observed significant horizontal motion of 7 mm between epochs one and two. Therefore, we excluded this station from our reference network for displacement analysis of the monitoring stations.

Table 3. GPS horizontal displacement from the reference network during the 16 month time interval between the first and the fourth campaign with 95% confidence interval.

Point Name	Epoch 1 to 2 (5 Months)		Epoch 2 to 3 (3 Months)		Epoch 3 to 4 (8 Months)	
	E-W (mm)	N-S (mm)	E-W (mm)	N-S (mm)	E-W (mm)	N-S (mm)
BM1	0 ± 1	0 ± 1	0 ± 5	0 ± 7	0 ± 5	0 ± 8
BM2	−2 ± 2	0 ± 2	1 ± 5	0 ± 7	0 ± 5	−1 ± 8
BM3	−6 ± 1	−4 ± 2	−3 ± 7	2 ± 9	4 ± 7	−5 ± 9

Performing four epochs of repeated GPS observations on a monitoring network also did not reveal any significant deformation on the Sarcheshmeh slope from October 2010 to April 2012 (Table 4). Figure 11 is a schematic display of an average horizontal displacement field map resulting from the first and the fourth campaign on the Sarcheshmeh slope. GPS horizontal displacement vectors for most of the stations do not show significant displacement at 95% confidence intervals. According to results in Table 4, all GPS stations were stable during the observed time interval. The only exceptions are MP.13 and MP.14, which showed significant horizontal motions of up to 1 cm and 14 cm, respectively, beyond the bounds of the estimated error ellipses (Figure 11 and Table 4). However, field check-ups performed following this observation indicated that the motion at these stations was not related to sliding of the entire slope but was locally triggered by human interference and water infiltration from nearby farming.

Figure 12 shows the displacement time series of some GPS stations (MP8, MP9, MP10 and MP17) corresponding to InSAR displacement time series (TS8, TS9, TS10 and TS17) illustrated in Figure 10. As clearly shown in Figure 12, the displacement values and plotted error bars are indicative of the station's stability.

Table 4. GPS horizontal displacement for monitoring stations with 95% confidence interval.

Point Name	Epoch 1 to 2 (5 Months)		Epoch 2 to 3 (3 Months)		Epoch 3 to 4 (8 Months)	
	E-W (mm)	N-S (mm)	E-W(mm)	N-S (mm)	E-W (mm)	N-S (mm)
MP1	−4 ± 4	−2 ± 6	−1 ± 4	3 ± 6	1 ± 4	2 ± 6
MP2	−1 ± 4	6 ± 4	−3 ± 6	−4 ± 6	4 ± 4	6 ± 6
MP3	−4 ± 4	−2 ± 4	−2 ± 12	−3 ± 14	4 ± 12	7 ± 14
MP4	−4 ± 4	0 ± 4	2 ± 6	1 ± 6	−3 ± 6	3 ± 8
MP5	4 ± 4	12 ± 4	−3 ± 4	−4 ± 6	2 ± 4	4 ± 6
MP6	−3 ± 2	3 ± 4	0 ± 2	0 ± 4	0 ± 4	1 ± 6
MP7	−4 ± 2	4 ± 4	0 ± 4	−4 ± 6	−3 ± 4	2 ± 8
MP8	−6 ± 6	4 ± 8	−5 ± 4	−1 ± 6	2 ± 4	1 ± 6
MP9	−1 ± 2	−3 ± 4	−2 ± 4	−4 ± 10	2 ± 4	7 ± 10
MP10	−7 ± 6	−1 ± 6	2 ± 4	3 ± 4	−3 ± 4	1 ± 4
MP11	−3 ± 4	1 ± 4	−2 ± 4	−1 ± 4	1 ± 4	−1 ± 4
MP12	−2 ± 4	2 ± 4	0 ± 4	−3 ± 6	−3 ± 4	4 ± 6
MP13	−9 ± 2	6 ± 4	−6 ± 2	−1 ± 4	−5 ± 2	6 ± 4
MP14	−4 ± 2	1 ± 4	130 ± 2	57 ± 4	25 ± 2	17 ± 4
MP15	−2 ± 2	−2 ± 4	−1 ± 4	2 ± 8	−2 ± 4	2 ± 8
MP16	−5 ± 2	1 ± 6	2 ± 4	2 ± 6	−6 ± 4	−3 ± 4
MP17	−1 ± 4	0 ± 4	−4 ± 4	−1 ± 6	2 ± 4	4 ± 6

Figure 11. Schematic display of an average horizontal displacement field on the Sarcheshmeh slope spanning the first and the fourth GPS campaign with 95% confidence ellipses.

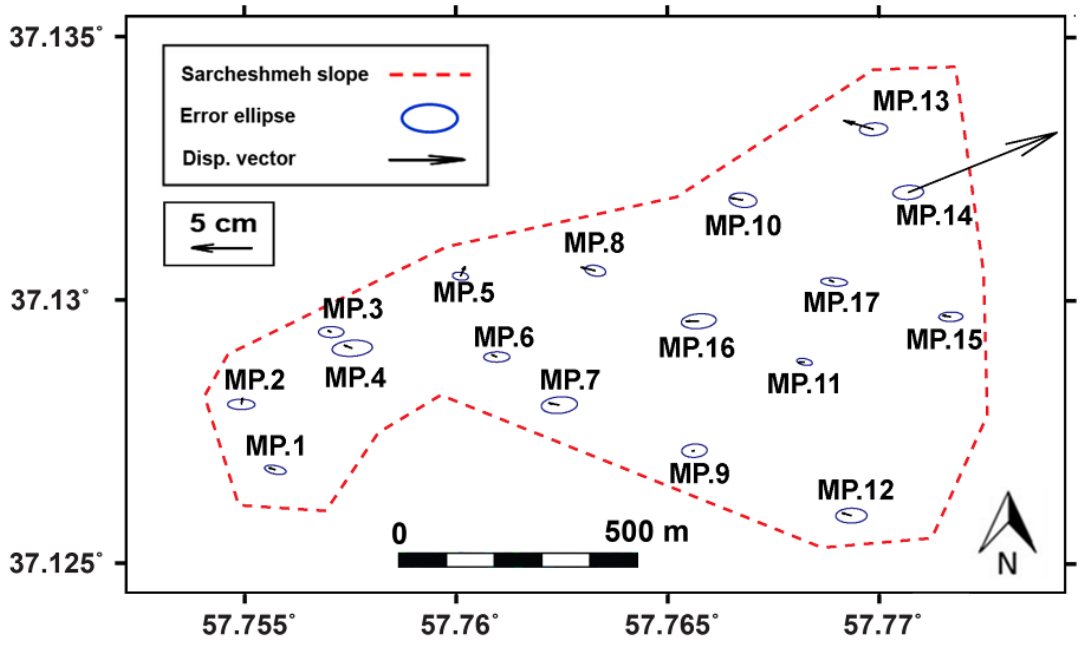

Figure 12. Four samples of GPS results with 95% error bars; for the location of points please see Figure 11. The solid circles represent displacement values, and the dashed blue line is a one-dimensional polynomial trend fitted to the displacement value.

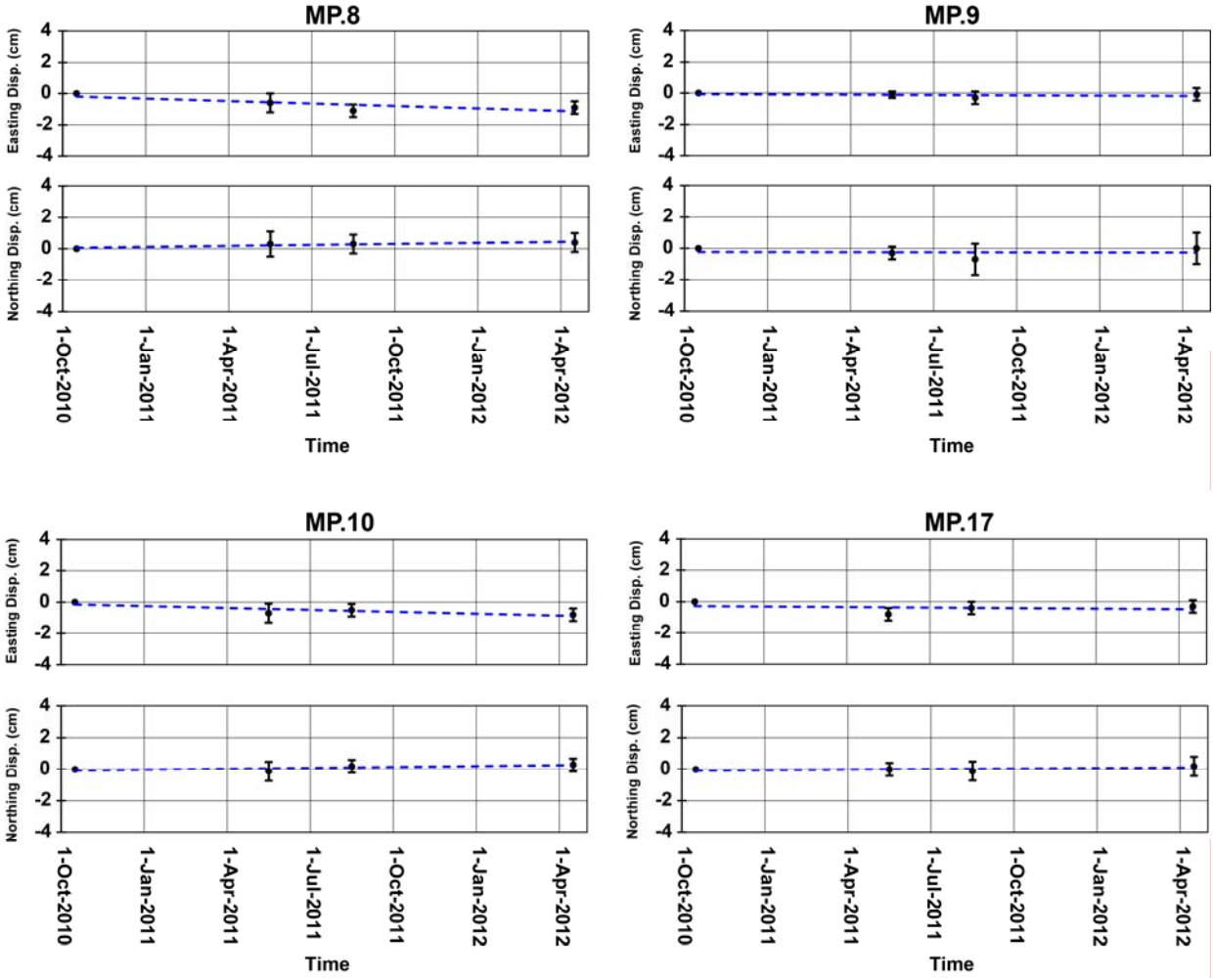

4. Discussion

In this study, InSAR was applied to Envisat data to assess the history of surface deformation on the Sarcheshmeh landslide, and repeated GPS campaign measurements were performed to assess the rate of surface deformation in the area. Although both methods were implemented in different time intervals, both indicate current stability of the Sarcheshmeh slope.

Standard errors analysis in GPS measurement does not show significant displacement on the landslide at 95% confidence interval. As shown in Figure 12, the cumulative displacement for most of the GPS stations on the landslide during the 2010–2012 time interval falls within the bounds of the estimated error ellipse; the only exceptions were MP.13 and MP.14 which were affected by localized deformation. The large uncertainty of the estimated displacements may arise from the limited number of campaign-mode measurements that we used in this study. The uncertainties of site displacements decrease if more repeat GPS surveys are performed to span longer times or we use continuous GPS instead of campaign-mode measurements [43].

For the InSAR investigation, the main limitations of C-band repeat-pass interferometry to reliably evaluate the long-term creep rate over the Sarcheshmeh landslide are atmospheric artifacts in interferograms with short temporal baselines and temporal decorrelation in interferograms with long time intervals (~1 year); the area is mountainous, partially covered with grass and other permanent vegetation and is used for farming, all of which contribute to the disturbance of the InSAR signal. However, SBAS time-series analysis using Envisat data enables identification of more than 600 coherent pixels that illustrate slope stability in the years 2004–2006 within the error threshold of InSAR observations. The mean deformation rate of the slope with respect to the reference area selected on the residential area downslope is estimated at 1.2 ± 4 mm/year. However, as the main direction of the landslide is towards the NW, any coherent motion related to landslide would have appeared as negative LOS in descending InSAR results. The positive value for the mean deformation and its relatively large uncertainty is an indication of the large impact of residual tropospheric effects on InSAR time-series analysis that compromises the precision of the derived deformation signal using a limited number of SAR images used in this study [44].

The Sarcheshmeh slope has been characterized as an ancient creeping hillside. Cluttered topography and the existence of scarps, trenches and deep grooves (Figure 3) are all geologically indicative of the creeping history of this slide. This area is located on a vast, massive limestone (Figure 2); thus, creeping can be facilitated by the groundwater level and high precipitation rate among other factors. Surface water can loosen dry soil and make sliding easier on the slippery bedrock. Water penetration also leads to slope overloading and increased slope weight. Therefore, gravity can interact more strongly in downward creeping, especially on weakly consolidated masses. The current stability of the Sarcheshmeh landslide might result from a combined reduction in the ground water levels and precipitation rate. Sarcheshmeh is in an area in Iran with a relatively high level of groundwater and high rate of seasonal precipitation. Multiple springs on and around the slope are indicative of relatively high levels of groundwater.

However because of regional population growth, the expansion of agricultural activity and, subsequently, the irregular use of underground water resources, this area has been subject to tangible reduction in groundwater level over the last few decades. Figure 13a shows a watershed basin segmentation map of North Khorasan. Different colors in Figure 13b are indicative of the groundwater level status of the segments. As shown in this figure, the Esfarayen basin is in a critical forbidden area from the groundwater level aspect because of irregular water extraction. The Sarcheshmeh slope, marked by a green dot in Figure 13a, is in the Esfarayen basin; from 1993 to 2010, the average level of ground water in the basin to which the Sarcheshmeh slope belongs has declined more than 13 m (Figure 13c). Additionally, the precipitation rate has also decreased by more than 30% during 2004–2007 (Figure 14). All of these factors might have contributed to the increased resistance of the slope to downward motion.

Despite the recent stability of the Sarcheshmeh slope, our GPS results indicate that human-induced farming activity might trigger sudden motion on this slope. As mentioned in the GPS results section, at two stations, namely MP.13 and MP.14, we recorded significant horizontal movement during our GPS campaigns. Field check-ups revealed that the motion on these stations was due to the development of a new farmland nearby. This farmland was irrigated manually from groundwater resources, facilitating the penetration of water to creep-prone masses. Therefore, saturated weak consolidated soil became

heavy and slippery and started to move downward because of gravity. If similar practices become widespread, this accidental event and its consequences, which result from human interference, can be a critical warning regarding the Sarcheshmeh slope. Current geodetic investigation shows that this ancient landslide is primarily dormant in the current period. However, even in the absence of major triggering factors such as earthquakes and heavy rainfall, the landslide can be reactivated by other factors, such as water infiltration from farming. Therefore, preventive measures and subsequent proceedings are still necessary to mitigate and reduce probable losses and causalities. The development of a surface and subsurface drainage system to control and conduct runoff outside the slope, construction of a new residential area in a safe area far from the landslide zone and establishment of an early warning system to provide information concerning critical moments are some executable plans to mitigate any damages.

Figure 13. (**a**) Watershed basin segmentation map of the North Khorasan province. The red polygon delineates the watershed basin of Esfarayen to which the Sarcheshmeh slope belongs; (**b**) groundwater level status of each basin in the North Khorasan province indicated using different colors; (**c**) Groundwater level diagram of the Esfarayen basin which shows significant reduction from 1993 to 2010 [45].

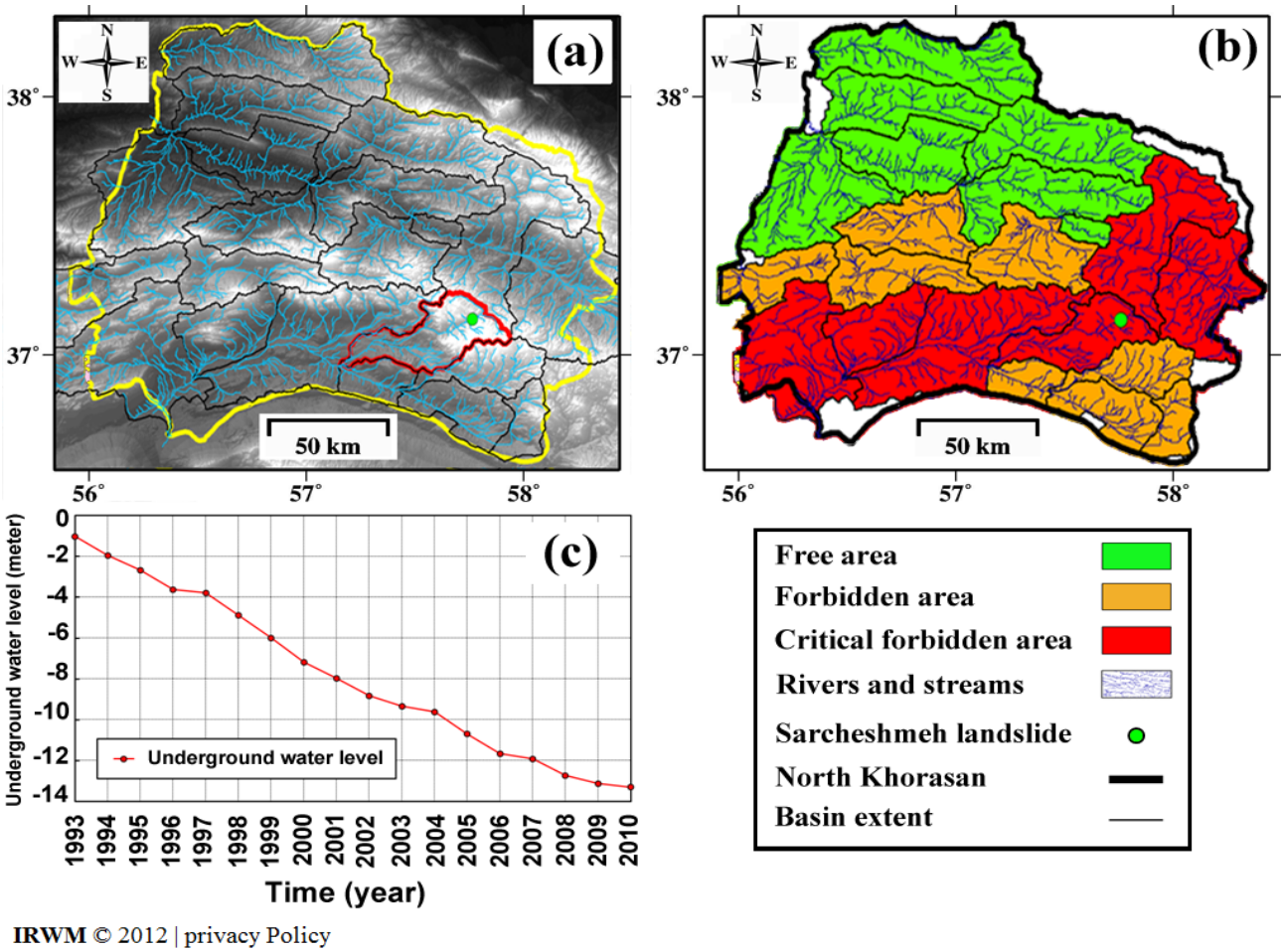

Figure 14. Accumulated monthly precipitation in Sarcheshmeh during 2004–2007 [12].

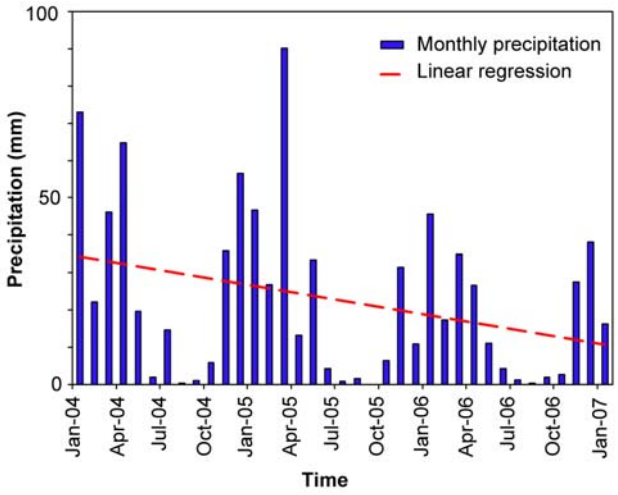

5. Conclusion

In this study, time-series analysis of Envisat InSAR data and repeated GPS observations using campaign measurements were employed to assess the slope stability of the Sarcheshmeh ancient landslide in Northeast Iran. No previous studies have examined the past and most recent movement of this landslide, and as a result its creeping mechanism was poorly understood. We were able to perform InSAR time-series analysis using Envisat data and detected more than 600 coherent pixels on the landslide, which showed no statistically significant LOS motion in the years 2004–2006. Horizontal campaign GPS data collected between 2010 and 2012 at 17 stations did not reveal any significant site motions within the estimated error ellipse of GPS results either. We interpret these results as indicating that the Sarcheshmeh landslide is currently inactive. Hydrological analysis suggests that the current dormancy of the landslide might be due to the absence of hydrological triggering factors in the region over the last decade.

Although the InSAR and GPS results in this paper are promising, we find that the uncertainty and precision of the results hamper our ability to detect and analyze the very slow creep signal in this region (<2–3 mm/year). Part of this uncertainty arises from not enough sampling of the slow creep signal in time in both Envisat data with 35-day repeat interval and campaign-mode GPS measurements. For future research, higher temporal and spatial resolution monitoring using observations from new SAR data such as TerraSAR-X (with a resolution of 1–3 m and a repeat time of 11 days) and placing continuously recording GPS sites in the landslide area are recommended. This would allow for more detailed sampling of deformation signal in time and space, in turn mitigating better the atmospheric and noise effects for evaluating slow landslide creep, and improvement of our capability to analyze the magnitude and seasonal dependence of a potential landslide motion in response to triggering conditions.

Acknowledgments

This work was supported by Initiative and Networking Fund of the Helmholtz Association in the frame of Helmholtz Alliance “Remote Sensing and Earth System Dynamics” and the German Federal

Ministry of Research and Technology (BMBF) within the framework of PROGRESS (Potsdam Research Cluster for Georisk Analysis, Environmental Change and Sustainability). It is a pleasure to thank those people who made this research possible, especially those who participated in the GPS field observations. We also thank the Forest, Range and Watershed Management (FRWM) organization of Iran for their support during this research project. Special thanks go to Bahman Akbari for initiating the project and to Mrs. Mohammadi and Fereydoun Masoumpour who graciously helped with the preparation of our field work. SAR data were provided by the European Space Agency (ESA) via proposal AOALO3740. Copyrights of Figures 1, 2b and 13c belong to National Geoscience Database of Iran, Geological Survey of Iran and Iran Water Resources Management Company, respectively. We are grateful to three anonymous reviewers and guest editor, Marco Scaioni, whose comments greatly improved the quality of the manuscript.

Conflict of Interest

The authors declare no conflict of interest.

References

1. Sidle, R.C.; Ochiai, H. *Landslides: Processes, Prediction, and Land Use*; American Geophysical Union: Washington, DC, USA, 2006; Volume 18, p. 312.
2. *Landslide in Iran*. Available online: http://landslide.ir (accessed on 20 December 2012).
3. *National Geoscience Database of Iran*. Available online: http://www.ngdir.ir/landslide/LandSlideInfo.asp (accessed on 20 December 2012).
4. Greif, V.; Vlcko, J. Monitoring of post-failure landslide deformation by the PS-InSAR technique at Lubietova in Central Slovakia. *Environ. Earth Sci.* **2012**, *66*, 1585–1595.
5. Malet, J.-P.; Maquaire, O.; Calais, E. The use of Global Positioning System techniques for the continuous monitoring of landslides: Application to the Super-Sauze earthflow (Alpes-de-Haute-Provence, France). *Geomorphology* **2002**, *43*, 33–54.
6. Brückl, E.; Brunner, F.; Kraus, K. Kinematics of a deep-seated landslide derived from photogrammetric, GPS and geophysical data. *Eng. Geol.* **2006**, *88*, 149–159.
7. Delacourt, C.; Allemand, P.; Berthier, E.; Raucoules, D.; Casson, B.; Grandjean, P.; Pambrun, C.; Varel, E. Remote-sensing techniques for analysing landslide kinematics: A review. *Bull. Soc. Geol. Fr.* **2007**, *178*, 89–100.
8. Strozzi, T.; Ambrosi, C.; Raetzo, H. Interpretation of aerial photographs and satellite SAR interferometry for the inventory of landslides. *Remote Sens.* **2013**, *5*, 2554–2570.
9. Kimura, H.; Yamaguchi, Y. Detection of landslide areas using satellite radar interferometry. *Photogramm. Eng. Remote Sensing* **2000**, *66*, 337–344.
10. Lacroix, P.; Zavala, B.; Berthier, E.; Audin, L. Supervised method of landslide inventory using panchromatic SPOT5 images and application to the earthquake-triggered landslides of Pisco (Peru, 2007, Mw8.0). *Remote Sens.* **2013**, *5*, 2590–2616.
11. Othman, A.A.; Gloaguen, R. River courses affected by landslides and implications for hazard assessment: A high resolution remote sensing case study in NE Iraq–W Iran. *Remote Sens.* **2013**, *5*, 1024–1044.

12. National Aeronautics and Space Administration. *Rainfall Analysis Tools*. Available online: http://disc2.nascom.nasa.gov/Giovanni/tovas/rain.GPCP.2.shtml (accessed on 11 January 2013).
13. *Water Science*. Available online: http://waterscience.blogfa.com (accessed on 20 December 2012).
14. Geological Survey of Iran. *States Information*. Available online: http://gsi.ir/States/Lang_en/StateId_51/Action_LastUpdate/index.html (accessed on 25 June 2011).
15. Hanssen, R.F. *Radar Interferometry: Data Interpretation and Error Analysis*; Kluwer Academic Publishers: New York, NY, USA, 2001.
16. Massonnet, D.; Feigl, K.L. Radar interferometry and its application to changes in the Earth's surface. *Rev. Geophys.* **1998**, *36*, 441–500.
17. Strozzi, T.; Farina, P.; Corsini, A.; Ambrosi, C.; Thüring, M.; Zilger, J.; Wiesmann, A.; Wegmüller, U.; Werner, C. Survey and monitoring of landslide displacements by means of L-band satellite SAR interferometry. *Landslides* **2005**, *2*, 193–201.
18. Tantianuparp, P.; Shi, X.; Zhang, L.; Balz, T.; Liao, M. Characterization of landslide deformations in three gorges area using multiple InSAR data stacks. *Remote Sens.* **2013**, *5*, 2704–2719.
19. Motagh, M.; Wetzel, H.-U.; Roessner, S.; Kaufmann, H. A TerraSAR-X InSAR study of landslides in southern Kyrgyzstan, Central Asia. *Remote Sens. Lett.* **2013**, *4*, 657–666.
20. Rott, H.; Scheuchl, B.; Siegel, A.; Grasemann, B. Monitoring very slow slope movements by means of SAR interferometry: A case study from a mass waste above a reservoir in the Ötztal Alps, Austria. *Geophys. Res. Lett.* **1999**, *26*, 1629–1632.
21. Hooper, A.; Zebker, H.; Segall, P.; Kampes, B. A new method for measuring deformation on volcanoes and other natural terrains using InSAR persistent scatterers. *Geophys. Res. Lett.* **2004**, *31*, doi: 10.1029/2004GL021737.
22. Hooper, A.; Segall, P.; Zebker, H. Persistent scatterer interferometric synthetic aperture radar for crustal deformation analysis, with application to Volcán Alcedo, Galápagos. *J. Geophys. Res.* **2007**, *112*, doi: 10.1029/2006JB004763.
23. Tofani, V.; Raspini, F.; Catani, F.; Casagli, N. Persistent Scatterer Interferometry (PSI) technique for landslide characterization and monitoring. *Remote Sens.* **2013**, *5*, 1045–1065.
24. Berardino, P.; Fornaro, G.; Lanari, R.; Sansosti, E. A new algorithm for surface deformation monitoring based on small baseline differential SAR interferograms. *IEEE Trans. Geosci. Remote Sens.* **2002**, *40*, 2375–2383.
25. Lanari, R.; Casu, F.; Manzo, M.; Zeni, G.; Berardino, P.; Manunta, M.; Pepe, A. An overview of the small baseline subset algorithm: A DInSAR technique for surface deformation analysis. *Pure Appl. Geophys.* **2007**, *164*, 637–661.
26. Akbari, V.; Motagh, M. Improved ground subsidence monitoring using small baseline SAR interferograms and a weighted least squares inversion algorithm. *IEEE Geosci. Remote Sens. Lett.* **2012**, *9*, 437–441.
27. Hofmann-Wellenhof, B.; Lichtenegger, H.; Collins, J. *Global Positioning System. Theory and Practice*; Springer: Wien, Austria, 1993; p. 347.
28. Zhou, P.; Zhou, B.; Guo, J.; Li, D.; Ding, Z.; Feng, Y. A demonstrative GPS-aided automatic landslide monitoring system in sichuan province. *J. Glob. Position. Syst.* **2005**, *4*, 184–191.
29. Gili, J.A.; Corominas, J.; Rius, J. Using Global Positioning System techniques in landslide monitoring. *Eng. Geol.* **2000**, *55*, 167–192.

30. Squarzoni, C.; Delacourt, C.; Allemand, P. Differential single-frequency GPS monitoring of the La Valette landslide (French Alps). *Eng. Geol.* **2005**, *79*, 215–229.
31. Motagh, M.; Djamour, Y.; Walter, T.R.; Wetzel, H.U.; Zschau, J.; Arabi, S. Land subsidence in Mashhad Valley, northeast Iran: Results from InSAR, levelling and GPS. *Geophys. J. Int.* **2006**, *168*, 518–526.
32. Yin, Y.; Zheng, W.; Liu, Y.; Zhang, J.; Li, X. Integration of GPS with InSAR to monitoring of the Jiaju landslide in Sichuan, China. *Landslides* **2010**, *7*, 359–365.
33. Strozzi, T.; Delaloye, R.; Kääb, A.; Ambrosi, C.; Perruchoud, E.; Wegmüller, U. Combined observations of rock mass movements using satellite SAR interferometry, differential GPS, airborne digital photogrammetry, and airborne photography interpretation. *J. Geophys. Res.* **2010**, *115*, doi: 10.1029/2009JF001311.
34. Kampes, B.; Hanssen, R.; Perski, Z. Radar Interferometry with Public Domain Tools; In Proceedings of FRINGE, ESA ESRIN, Frascati, Italy, 1–5 December 2003; Available online: http://earth.esa.int/fringe03/proceedings/papers/22_kampes.pdf (accessed on 25 May 2013).
35. Farr, T.G.; Kobrick, M. The shuttle radar topography mission. *Rev. Geophys.* **2007**, *45*, doi: 10.1029/2005RG000183.
36. Scharroo, R.; Visser, P. Precise orbit determination and gravity field improvement for the ERS satellites. *J. Geophys. Res.* **1998**, *103*, 8113–8127.
37. Hooper, A. A multi-temporal InSAR method incorporating both persistent scatterer and small baseline approaches. *Geophys. Res. Lett.* **2008**, *35*, doi: 10.1029/2008GL034654.
38. National Geodetic Survey. *GPS Orbit Data*. Available online: http://www.ngs.noaa.gov/orbits/orbit_data.shtml (accessed on 30 November 2012).
39. Wesche, C.; Eisen, O.; Oerter, H.; Schulte, D.; Steinhage, D. Surface topography and ice flow in the vicinity of the EDML deep-drilling site, Antarctica. *J. Glaciol.* **2007**, *53*, 442–448.
40. Lowry, A.R.; Hamburger, M.W.; Meertens, C.M.; Ramos, E.G. GPS monitoring of crustal deformation at Taal Volcano, Philippines. *J. Volcanol. Geotherm. Res.* **2001**, *105*, 35–47.
41. Hessami, K.; Nilforoushan, F.; Talbot, C.J. Active deformation within the Zagros mountains deduced from GPS measurements. *J. Geol. Soc.* **2006**, *163*, 143–148.
42. McClusky, S.; Balassanian, S.; Barka, A.; Demir, C.; Ergintav, S.; Georgiev, I.; Veis, G. Global Positioning System constraints on plate kinematics and dynamics in the eastern Mediterranean and Caucasus. *J. Geophys. Res.-Solid Earth* **2000**, *105*, 5695–5719.
43. Langbein, J. Noise in GPS displacement measurements from Southern California and Southern Nevada. *J. Geophys. Res.-Solid Earth* **2008**, *113*, doi: 10.1029/2007JB005247.
44. Casu, F.; Manzo, M.; Lanari, R. A quantitative assessment of the SBAS algorithm performance for surface deformation retrieval from DInSAR data. *Remote Sens. Environ.* **2006**, *102*, 195–210.
45. Iran Water Resources Management Company. *North Khorasan Province*. Available online: http://wnkh.ir/showpage.aspx?pgid=8&ids=29&? (accessed on 11 January 2013).